Parametric Identification of an Experimental Magneto-Elastic Oscillator

B. F. FEENY
Michigan State University
Department of Mechanical Engineering
East Lansing, MI 48824 USA

C.-M. YUAN
Chun Shan Institute of Science and Technology
P.O. Box 90008-6-16
Lungtan, 325, Taiwan ROC

J. P. CUSUMANO
Pennsylvania State University
Department of Engineering Science and Mechanics
State College, PA 16801 USA

Abstract

The identification of parameters in an experimental two-well chaotic system is presented. The method involves the extraction of periodic orbits from a chaotic set. The form of the differential-equation model is assumed, with unknown coefficients on the terms in the model. The harmonic-balance method is applied to these periodic orbits, resulting in a linear equation in the unknown parameters, which can then be solved in the least-squares sense. The identification process reveals the nonlinear force-displacement characteristic of the oscillator. The results are cross-checked with various sets of extracted periodic orbits. The model is validated by comparing the linearized characteristics, examining simulated responses, and evaluating the vector field.

1. Introduction

System identification can be broadly divided into nonparametric identification and parametric identification. In parametric system identification, enough is known *a priori* to write the form of the differential equations of motion, although with unknown coefficients multiplying linear and/or nonlinear functions in these equations. Among the many methods for nonlinear parametric identification are those of Nayfeh [1], in which resonances are exploited, Stry and Mook [2], which is applied to the time series, Gottlieb *et al.* [3] and Feldman [4], which employ the Hilbert transform, and Yasuda *et al.* [5, 6], in which the harmonic-balance method is used in an inverse way to estimate parameters.

One of the applications of chaos is in system modeling. To this end, much of the activity is geared toward dimensionality studies, in which bounds on the number of active state variables are established. The determination of the size of a system might be a first step in developing *a priori* knowledge that may later be used in parametric system identification. In addition, nonlinear prediction can be performed using modern methods of analyzing chaotic data [7].

The fundamental property of deterministic chaos that we exploit is that a chaotic set is the closure of infinitely many unstable periodic orbits. Poincaré (1854-1912) realized the existence of periodic orbits within the complex tangles of the three-body problem, and their potential

usefulness: "These periodic solutions are so valuable for us because they are, so to say, the only breach by which we may attempt to enter an area heretofore deemed inaccessible." (The quote is obtained through Tufillaro *et al.* [8].)

Indeed the unstable periodic orbits can be approximately extracted from chaotic data from either discrete or continuous-time systems [8, 9, 10]. They have been used in system identification, usually in the Poincaré section [11, 12, 13]. The harmonic balance method has been used with the unstable periodic orbits in a variety of numerical test cases, including autonomous and non-autonomous oscillators [14]. An error analysis showed that the usage of many periodic orbits gives a more reliable fit of the parameters than a single periodic orbit. The drawback is that the extracted unstable periodic orbits are approximations, not only due to the usual errors of experimental observation, but also since the recursive orbit represents a trajectory in the neighborhood of a saddle-type periodic orbit.

In this paper, we investigate a chaotic data set taken from a periodically driven magneto-mechanical oscillator with a two-well potential. The harmonic-balance parametric-identification scheme is applied to chaotic data of this experimental system. The chaotic attractor is reconstructed using the method of delays [15, 16], from which the unstable periodic orbits are extracted for use in the identification algorithm. A mathematical model is chosen first in polynomial form by knowing that the experimental system has a smooth two-well stiffness potential, and then in the form of interpolation functions. The method of harmonic balance is used to form a set of algebraic equations in system parameters, which are estimated by a least-squares fit.

The next section includes a description of the experiment, and the process of obtaining experimental periodic orbits. Section 3 focuses on the identification of parameters in models of the system. Section 4 addresses the verification of the identified models, and also damping issues. Conclusions are drawn in Section 5.

2. Experiments

Here we describe the experimental system and the process of obtaining periodic data needed for the identification scheme.

2.1. Experimental Setup

The experiment consisted of a stiffened beam buckled by two magnets (Figure 1). Two rare-earth permanent magnets were placed on the base of the frame holding the beam to create the two-well potential. The beam had extra rigidity in the form of steel bars epoxied and bolted along the length away from the clamped end. This additional rigidity was included to make the system behave as a single degree of freedom. The fruit of this effort includes the recovery of the stable and unstable manifolds by means of stochastic interrogation [17]. The uncovered portion of the beam near the clamped end acted as an elastic hinge from which the position of the beam was measured by strain gauges. The frame was then fixed through a rigid mount to an electromagnetic shaker. A periodic driving signal was fed through a power amplifier to the shaker to provide the external forcing function.

Data from the strain gauges were acquired using a 12-bit, ± 5 V data-acquisition (A/D) board, with the digital values from -2048 to 2047 corresponding to -5 V to 5 V. With no forcing, three equilibria exist: two are stable at digital values of -495 and 315 (-1.21 V and

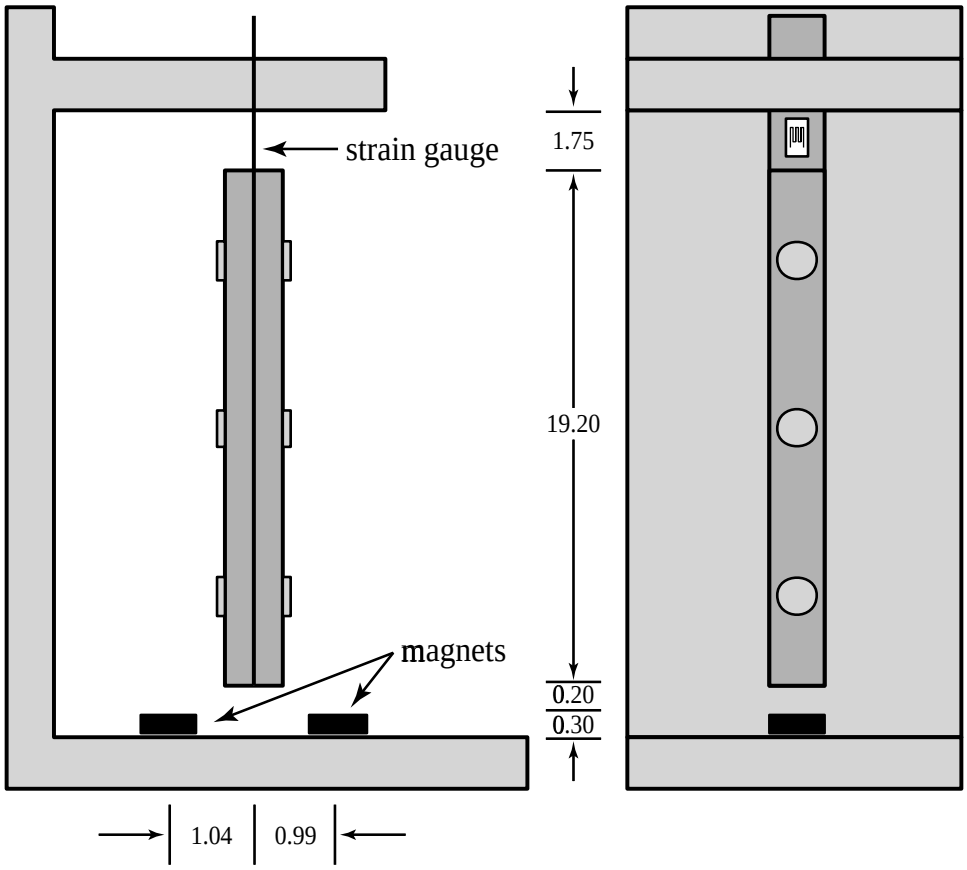

Figure 1: Experimental set-up. Lengths are in cm.

0.77 V), and one is unstable (saddle) at approximately zero. The driving frequency was set at 7.5 Hz with 1.5 V of the function generator output, by which the chaotic data were generated, passed through a 50 Hz low-pass filter, and collected at the sampling frequency of 187.5 Hz for 7000 periods of excitation. At this sampling frequency and driving frequency, there are 25 samples per driving period.

2.2. Phase-Space Reconstruction

Since there is only one observable in the data set, denoted by $\{x_j\}, j = 1, \ldots, N$, with $x_j = x(j\Delta t)$, where x is the displacement of the beam tip and Δt is the sampling time interval, the phase space of the experimental system is to be reconstructed using the method of delays [15, 16] to build d-dimensional pseudo vectors with elements being the single observable separated by a constant delay time, such that $\mathbf{y}_j = (x_j, x_{j+\tau}, \cdots, x_{j+\tau(d-1)})$, where τ is the delay index, and d is embedding dimension, both of which are to be determined. The pseudo-vector represents a data point in the pseudo phase space. We chose $\tau = 7$ samples based on the first minimum in the average mutual information [18] between x_n and $x_{n+\tau}$ as τ increases. The average mutual information was computed on a grid generated from 40 equally sized bins in each axis. The data were then reconstructed in a four-dimensional delay space. The four dimensions were determined by singular systems analysis [19] with $\tau = 2$ and by the method

of false nearest neighbors [20] with $\tau = 7$.

2.3. Periodic-Orbit Extraction

From the reconstructed chaotic attractor, the unstable periodic orbits can be extracted as follows [8, 10]. In the pseudo phase space, we seek recurrent points such that

$$|\mathbf{y}_{i+K} - \mathbf{y}_i| \leq \epsilon, \tag{1}$$

where K is an integer and ϵ is set as 1.75 % of the maximum extent of the chaotic set. The actual recurrence errors on the extracted orbits ranged from 0.51 % to 1.73 %.

There is some art in choosing the parameter ϵ. If ϵ is too small, then insufficient recurrences will be detected. If ϵ is too large, then the recurrent orbits may not faithfully represent the unstable periodic orbits. A bound on the error at the recurrence is proportional to ϵ, with the proportionality dependent on the local linear dynamics about the unstable periodic orbit [14]. Examples of the effects of ϵ on recurrence errors, and full-orbit errors, were examined by Al-Zamel [21]. Effects of ϵ on errors in Fourier coefficients have not been examined in detail. A value of $\epsilon = 0.5\%$ of the span of the data was used in references [8, 10].

Researchers often collect several extractions of an unstable periodic orbit and use the average as its representation. With our data set, and our choice of ϵ, we find few repetitions of periodic orbits. Also, it has been observed that orbits with the minimum recurrence tend to be the most accurate [21]. Therefore, we do not take averages to represent periodic orbits.

3. Parameter Identification

The identification process involves the choice of a mathematical model with parameters in the form of unknown coefficients. Once periodic orbits are available, the harmonic balance method is then performed on function evaluations of the periodic displacements. Parameters are determined in the least-squares sense.

3.1. Choosing a Mathematical Model

Knowing that the experimental system is an externally excited nonlinear system with a two-well potential, we first choose a mathematical model in a polynomial form to fit the characteristics of the nonlinear function. We choose a polynomial because we know that the magnetic and elastic forces are smooth. We do not know, however, whether a power series converges to the actual stiffness characteristic in the domain of the displacement. Furthermore, in the case of divergence, we do not know the optimal truncation of the series representation. Our best hope is to obtain a model which qualitatively fits the characteristic of the experimental system. Later, we implement an interpolation model [22].

The general model with viscous damping is written as

$$m\ddot{x} + \alpha\dot{x} + \sum_{i=0}^{p} \beta_i f_i(x, \dot{x}) = a\cos\omega t + b\sin\omega t. \tag{2}$$

where p is the number of terms in the power series. For illustration, suppose $m = 1$ and α, β_i, a and b are the parameters to be determined. In the case of a polynomial stiffness model, we have $f_i(x, \dot{x}) = x^i$.

3.2. Harmonic Balance

We follow the identification scheme introduced by Yasuda *et al.* [5]. Given a measured periodic response in $x(t)$, which may be either stable or extracted from the chaotic attractor, the nonlinear functions, when evaluated with $x(t)$, are periodic and can be approximated in a truncated Fourier series, such as

$$x_k \approx \frac{a_0}{2} + \sum_{j=1}^{n} (a_j \cos\frac{j\omega t}{k} + b_j \sin\frac{j\omega t}{k}),$$

$$\dot{x}_k \approx \sum_{j=1}^{n} \frac{j\omega}{k} (b_j \cos\frac{j\omega t}{k} - a_j \sin\frac{j\omega t}{k}),$$

$$\ddot{x}_k \approx -\sum_{j=1}^{n} \frac{j^2\omega^2}{k^2} (a_j \cos\frac{j\omega t}{k} + b_j \sin\frac{j\omega t}{k}),$$

and

$$f_i(x_k, \dot{x}_k) = x_k^i \approx \frac{c_{i0}}{2} + \sum_{j=1}^{n} (c_{ij} \cos\frac{j\omega t}{k} + d_{ij} \sin\frac{j\omega t}{k}).$$

The subscript k indicates that the data is period-k. The Fourier coefficients are calculated from the data, which have a period $T = k\omega$. For the case of polynomial nonlinear functions, $c_{1j} = a_j$ and $d_{1j} = b_j$.

Substituting these Fourier series into the model equation (2), and balancing the Fourier coefficients of any set of harmonics, a set of *linear* algebraic equations in system parameters can be constructed. This usage of the harmonic-balance method contrasts its usual usage for response analysis, where the ordinary differential equation is known, and the effort is to solve a set of *nonlinear* equations in Fourier coefficients. For systems forced with a single harmonic, and for autonomous systems, the method of harmonic balance requires nonlinearity so that several harmonics can be balanced.

In this paper, we typically use multiples of the primary harmonic. Although subharmonics are also available, we have not implemented them. Thus, for the example of $m = 1$ and $k = 1$, the balance equations, in matrix form, are

$$\begin{bmatrix} 0 & c_{00} & c_{10} & \cdots & c_{p0} & 0 & 0 \\ \omega b_1 & c_{01} & c_{11} & \cdots & c_{p1} & -1 & 0 \\ -\omega a_1 & d_{01} & d_{11} & \cdots & d_{p1} & 0 & -1 \\ \vdots & \vdots & \vdots & & \vdots & \vdots & \vdots \\ n\omega b_n & c_{0n} & c_{1n} & \cdots & c_{pn} & 0 & 0 \\ -n\omega a_n & d_{0n} & d_{1n} & \cdots & d_{pn} & 0 & 0 \end{bmatrix} \begin{bmatrix} \alpha \\ \beta_0 \\ \beta_1 \\ \vdots \\ \beta_p \\ a \\ b \end{bmatrix} = \begin{bmatrix} 0 \\ \omega^2 a_1 \\ \omega^2 b_1 \\ \vdots \\ (n\omega)^2 a_n \\ (n\omega)^2 b_n \end{bmatrix}$$

or

$$\mathbf{A}\hat{\alpha} = \mathbf{q}, \tag{3}$$

where $\hat{\alpha}$ is the parameter vector of the system model, $\mathbf{A}$ is a $(2n+1) \times (p+4)$ matrix, $\mathbf{q}$ is a $(2n+1)$ vector containing the Fourier coefficients of the external forcing function, and n is the number of harmonics retained in the Fourier series representation. Each column of $\mathbf{A}$ contains the Fourier coefficients of the corresponding term in the system model. For general values of k,

the indices and frequencies in the elements of matrix $\mathbf{A}$ are scaled by k. The vector $\mathbf{q}$ contains a non-zero elements due to known quantities in the differential equations.

If any parameters are known, they can be incorporated into the known quantities in $\mathbf{q}$. By dividing through by m, we eliminate one parameter, and end up with a coefficient of '1' in front of the $\ddot{x}$ term. In such case, the $(n\omega)^2$ terms are incorporated into $\mathbf{q}$.

If $2n = p + 3$ and the matrix $\mathbf{A}$ is non-singular, the parameter vector α can be determined uniquely. In practice, it is statistically better if the algebraic equation (3) is over determined, so that $2n > p+3$. Consequently the exact solution will not generally exist, but a best solution can be obtained by a method such as a least-squares fit. This can be done by performing a pseudo inverse which involves singular decomposition. (See references [23, 24] for a geometric discussion, and [14] for previous application to this problem.)

Theoretically, the number of terms in the Fourier series should be infinite, but Mickens [25] has shown that the upper bounds of the absolute magnitudes of the harmonic coefficients decrease exponentially, such that they become ineffective in the least-squares estimation procedures. Another consideration is that our extracted orbits are approximately periodic, and the deviation from periodicity tends to show up as a small kink which registers in the higher harmonics. In our experience, the best results are obtained if n is from two to four, where n is the number of harmonics of the primary (driving) frequency. This limits the number of unknown parameters in the model that can be estimated using a single periodic orbit. (It might be worthwhile to investigate the use of subharmonics.) However, we can use several periodic orbits to form several sets of algebraic equations, thereby augmenting the matrix $\mathbf{A}$ to increase the redundancy of algebraic equations for the least-squares estimation. This treatment can improve estimation results even if the number of unknown parameters is not excessively large. This availability of several extracted periodic orbits from a chaotic set increases the applicability beyond that of a simple periodic response.

3.3. Data Processing Issues

The experimental data are in a digital format, ranging from -5 V to 5 V of the voltage output from the A/D converter. There is a scaling factor between the voltages and the displacement units. The parameters in equation (2) are scaled by this factor in a nonlinear fashion. We assume that the factor between the digital data z and the variable x in equation (2) is a constant γ in units of m/V, such that $x = \gamma z$. Substituting this into equation (2), the model equation can be rewritten as

$$(m\gamma)\ddot{z} + (\alpha\gamma)\dot{z} + \sum_{i=0}^{p}(\beta_i\gamma^i)z^i = a\cos\omega t + b\sin\omega t, \tag{4}$$

If the data are large in amplitude, the high-order nonlinear terms will be even larger in amplitude, causing an ill-conditioning of the matrix $\mathbf{A}$ used in the least-squares fit. To prevent this, we can choose γ in such a way as to normalize the data to the unit interval. We have, in fact, not normalized the data, since its absolute value is confined to a few volts, and the condition numbers for our matrix $\mathbf{A}$ are reasonable. The time variable, however, is nondimensionalized to a new variable, $\tilde{t} = \omega t$. This normalization of time is manifested in the velocity and acceleration terms, and improves the conditioning of the least-squares problem.

Meanwhile, we know that the external forcing is periodic, although the forcing amplitude is unknown. This implies that equation (4) is actually indeterminate. To handle this, we divide

Table 1: Fourier coefficients of three sets of unstable period-one orbits (UPOs) extracted from chaotic data, and three periods of a stable period-one response (SPOs). The periodic orbits are distinguished by their associated indices.

	UPOs			SPOs		
harmonic	$n = 51384$	$n = 51410$	$n = 51436$	$n = 100$	$n = 500$	$n = 1000$
DC term	0.7408	0.7355	0.7386	0.8067	0.8077	0.8079
$\cos t$	0.5072	0.4836	0.4598	-0.5724	-0.5725	-0.5725
$\sin t$	-0.6167	-0.6378	-0.6251	-0.1069	-0.1097	-0.1131
$\cos 2t$	-0.0146	-0.0048	-0.0076	-0.0079	-0.0080	-0.0087
$\sin 2t$	-0.0135	-0.0224	-0.0226	-0.0025	-0.0028	-0.0032
$\cos 3t$	0.0127	0.0133	0.0157	0.0063	0.0071	0.0069
$\sin 3t$	-0.0003	0.0061	0.0063	0.0049	0.0052	0.0055

through equation (4), written in terms of $\tilde{t}$, by the quantity $m\gamma\omega^2$, and recast it in the form

$$\tilde{\alpha}z' + \sum_{i=0}^{p} \tilde{\beta}_i z^i - \tilde{a}\cos\tilde{t} - \tilde{b}\sin\tilde{t} = -z'', \tag{5}$$

where the prime represents $d/d\tilde{t}$, and $\tilde{\alpha} = \alpha/m\omega$, $\tilde{\beta}_i = \beta_i\gamma^{i-1}/m\omega^2$, $\tilde{a} = a/m\gamma\omega^2$, and $\tilde{b} = b/m\gamma\omega^2$ are the parameters to be determined. Equation (5) fits the form of equation ().

Using the extracted periodic orbits, each term in the model equation (5) is nearly periodic and approximately expressed in a truncated Fourier series. The Fourier coefficients of the multiples of primary harmonics are balanced to form a set of algebraic equations in system parameters for least-squares estimations as previously described.

3.4. Errors in Extracted Periodic Orbits

Since we are balancing harmonics of the periodic orbits to identify parameters, it is of interest to investigate the errors that the extracted unstable periodic orbits have in their Fourier coefficients. To this end, we compare Fourier coefficients of extracted unstable periodic orbits with those of stable periodic responses. Table 1 contains the Fourier coefficients of three extractions of the same period-one response from the chaotic data. This set is compared with three arbitrarily chosen periods of a different, stable period-one response. In this case, the extracted period-one orbits are all part of the same visit to the unstable period-one orbit, and there is no time between the extracted orbits listed. On the other hand, the listed stable periodic orbits on not directly in sequence, rather there is some time between them. The comparison gives some sense of the variation inherited by the orbits as they are extracted from the chaotic set. This variation will be enhanced for velocity and acceleration signals, and will also be distorted in function evaluations of the signals.

Considerable variation is also observed in the primary Fourier coefficients of extracted periodic orbits of other periods. Some effort has been made to analytically estimate bounds on the errors in the Fourier coefficients due to errors in the periodic orbits [14, 26], and also to improve the extracted UPOs based on local dynamics [13, 26].

Table 2: Identification results for a cubic model with three primary harmonics balanced. Groups of ten unstable periodic orbits (UPOs) are displayed against the periodicities of the orbits used, and an estimation based on all thirty UPOs is also listed.

UPOs	$\tilde{\alpha}$	$\tilde{\beta}_0$	$\tilde{\beta}_1$	$\tilde{\beta}_2$	$\tilde{\beta}_3$	$\tilde{a}$	$\tilde{b}$
$1-10$	0.0068	0.0413	-0.2247	0.0621	0.1705	-0.1433	0.2481
$1-10$	-0.0197	-0.0377	-0.2421	0.1037	0.1840	-0.1750	0.2861
$2,4,4,5,6,6-10$	0.0153	-0.0565	-0.2719	0.1271	0.1935	-0.1945	0.2636
all UPOs	0.0057	-0.0251	-0.2424	0.1026	0.1825	-0.1750	0.2669

Table 3: Identification results for a cubic model with two primary harmonics balanced. Groups of ten unstable periodic orbits (UPOs) are displayed, and an estimation based on all thirty UPOs is also listed.

UPOs	$\tilde{\alpha}$	$\tilde{\beta}_0$	$\tilde{\beta}_1$	$\tilde{\beta}_2$	$\tilde{\beta}_3$	$\tilde{a}$	$\tilde{b}$
$1-10$	0.0034	0.0329	-0.2560	0.0709	0.1837	-0.1425	0.2425
$1-10$	-0.0359	-0.0477	-0.2894	0.1189	0.2062	-0.1683	0.2793
$2,4,4,5,6,6-10$	0.0041	-0.0621	-0.3005	0.1338	0.2045	-0.1903	0.2613
all UPOs	-0.0032	-0.0331	-0.2759	0.1125	0.1970	-0.1718	0.2619

3.5. Results for Polynomial Models

Using various sets of extracted periodic orbits together in the identification algorithm, with the data being processed as discussed above, and using the model equation (5), identification results are shown in Tables 2-4. Table 2 shows results for a cubic stiffness model, identified from the balance of three primary harmonics. The third harmonic of the primary frequency represents a frequency of 22.5 Hz, which is below the nominal filter frequency of 50 Hz. Table 3 lists the identified parameters when two primary harmonics are used. The variation seen in the parameters between two and three balanced harmonics is on par with the variation within the different sets of periodic orbits. Table 4 shows the parameters identified for a fourth-degree stiffness model with three primary harmonics balanced. In most cases the fourth degree coefficient is quite small. The coefficients of the other terms indicate an agreement between the identified fourth degree stiffness and the identified cubic stiffness.

In each case, there is some consistency in the damping coefficients, the forcing terms, and the qualitative nature of the identified stiffness. Somewhat disturbing are the incidences of negative damping. We will revisit this damping issue later. The three stiffness functions, each identified from thirty periodic orbits, are plotted in Figure 2. We will use the cubic model based on three primary harmonics of thirty unstable periodic orbits for the validation. Since the fourth-degree model is globally unstable, it is assumed to be a less-robust representation of the system. The cubic model identified from two harmonics produced a negative damping coefficient which is taken to be physically unrealistic.

Based on the results for 30 periodic orbits and three primary harmonics, we obtain a

Table 4: Identification results for a fourth-degree model with three primary harmonics balanced. Groups of ten unstable periodic orbits (UPOs) are displayed, and an estimation based on all thirty UPOs is also listed.

UPOs	$\tilde{\alpha}$	$\tilde{\beta}_0$	$\tilde{\beta}_1$	$\tilde{\beta}_2$	$\tilde{\beta}_3$	$\tilde{\beta}_4$	$\tilde{a}$	$\tilde{b}$
$1-10$	0.0070	0.0407	-0.2239	0.0636	0.1701	-0.0004	-0.1435	0.2483
$1-10$	-0.0324	-0.0788	-0.2259	0.1985	0.1708	-0.0624	-0.1707	0.2353
$2,4,4,5,6,6-10$	0.0121	-0.0314	-0.3555	0.0371	0.2288	0.0295	-0.2026	0.2633
all UPOs	0.0056	-0.0343	-0.2313	0.1260	0.1763	0.0070	-0.1748	0.2680

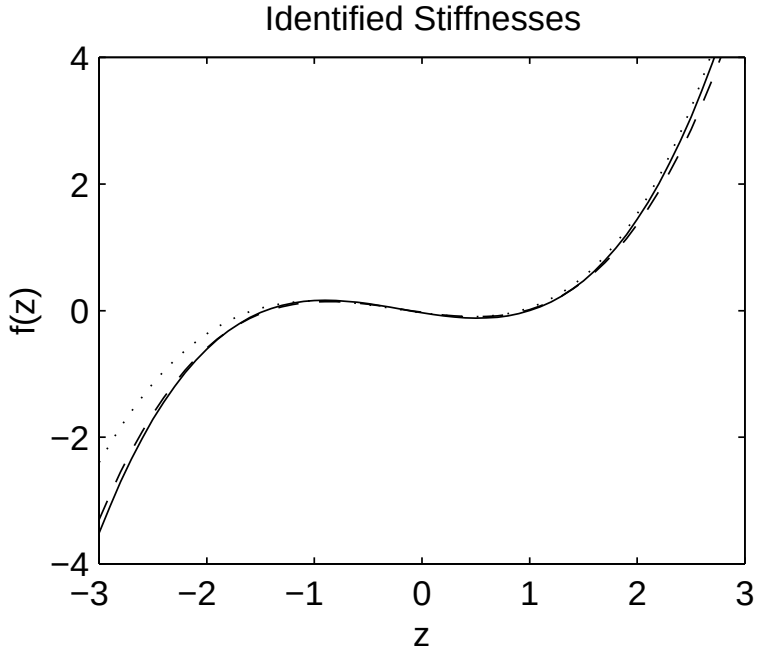

Figure 2: Plots of the identified stiffness models for a cubic polynomial from 30 unstable periodic orbits with three primary harmonics balanced (solid line), a cubic model with four harmonics balanced (dashed line), and a fourth-degree polynomial with three harmonics balanced.

qualitative model for the experimental system:

$$z'' + 0.0057z' - 0.0251 - 0.2424z + 0.1026z^2 + 0.1825z^3 = 0.3192\cos\tilde{t}. \tag{6}$$

Recall that the model is scaled from physical units by an unknown calibration factor γ.

3.6. Results for an Interpolation Model

We also used interpolation functions [22] to identify the system. The model was

$$z'' + \tilde{\alpha}z' + \sum_{i=1}^{N} \tilde{\beta}_i \phi_i(z) = \tilde{a}\cos\tilde{t} + \tilde{b}\sin\tilde{t}, \tag{7}$$

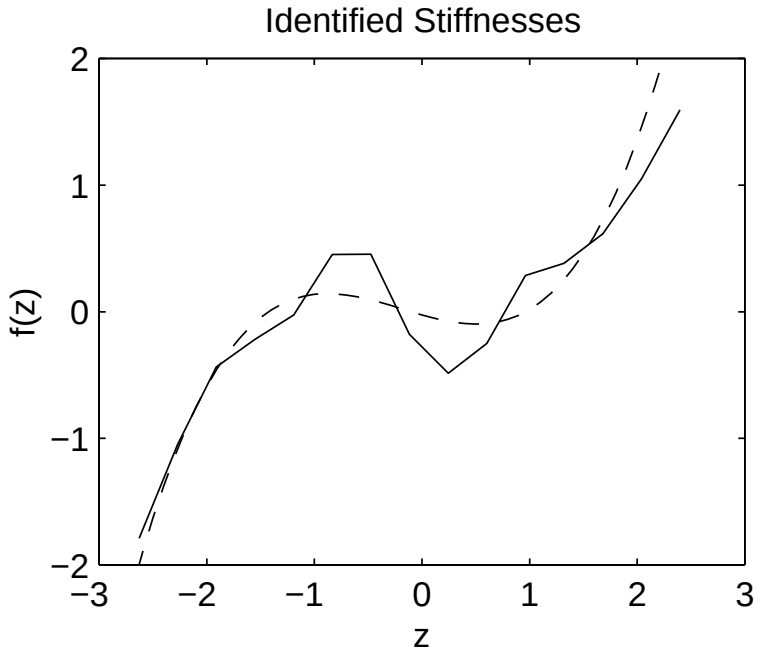

Figure 3: A plot of the identified nonlinear stiffness in terms of interpolation functions. Also plotted is the identified cubic model for comparison.

where $\phi_i(z)$ are localized tent functions, explained as follows. The span of the data, $s = \max(z) - \min(z)$, is split up into $N-1$ equal intervals (a_i, a_{i+1}), $i = 1, \ldots, N-1$, of length h. Then $\phi_i(z) = (z - a_i)/h$ if $a_{i-1} < z < a_i$, $\phi_i(z) = -(z - a_{i+1})/h$ if $a_i < z < a_{i+1}$, and $\phi_i(z) = 0$ otherwise. The $\phi_i(z)$ play the same role as each monomial in the polynomial model. The identification process is carried out the same way, such that the parameters $\tilde{\beta}_i$ are estimated. The relationship between the parameters in the voltage-unit, time-normalized coordinates, and those of the displacement coordinates which are not time normalized, may not be so clear. Nonetheless, the model in the normalized coordinates is useful for our purposes

The resulting interpolated stiffness model, based on $N = 15$, $n = 2$ primary harmonics and thirty periodic orbits, is plotted in Figure 3, and is compared to the cubic model based on thirty periodic orbits and $n = 3$. The integral of this stiffness force shows the identified two-well potential (Figure 4). The interpolation function reveals a two-well potential with slightly more localized features. These comparisons visually suggest how the cubic term represents a fit to the physical force characteristic.

The estimated damping coefficients $\tilde{\alpha}$ and force amplitudes are tabulated for several values of N and n in Table 5. The numbers are quite consistent with variation of N for a fixed value of n. Plots of the interpolated stiffness functions, though not shown, show a consistent shape for these values of N and n. Outside these values, the plots lose this consistency, and develop oscillations in z.

Next, these identified models are to be validated and compared.

4. Verification of the Identified Models

We evaluate the identified model by comparing the properties of the models linearized about

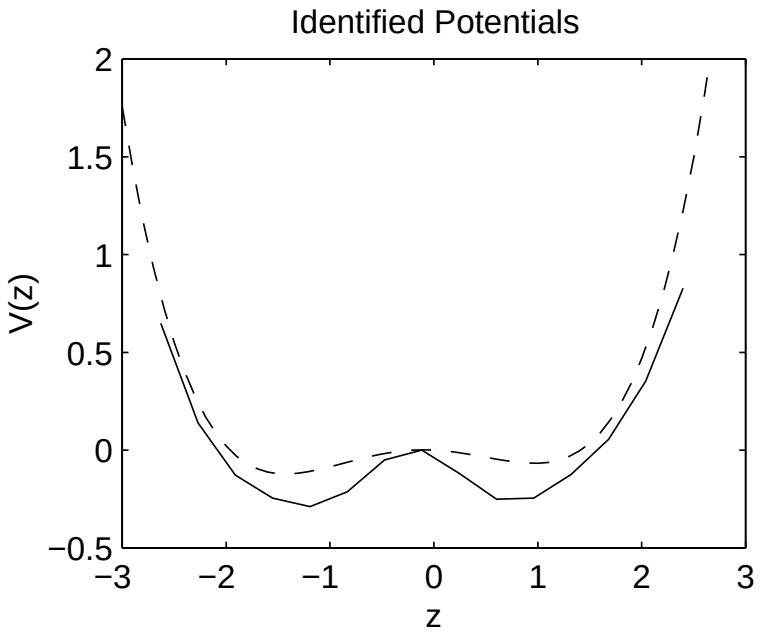

Figure 4: A plot of the identified two-well potential in terms of interpolation functions. Also plotted is the identified cubic model for comparison.

Table 5: Identified damping coefficients and forcing amplitudes for models based on N equally spaced interpolation functions ϕ_i, with n primary harmonics balanced among 30 unstable periodic orbits.

N	n	$\tilde{\alpha}$	$\sqrt{\tilde{a}^2+\tilde{b}^2}$
11	2	0.0179	0.2989
11	3	0.0113	0.2971
13	2	0.0197	0.2968
13	3	0.0111	0.2939
15	1	0.0228	0.3067
15	2	0.0184	0.2968
15	3	0.0077	0.2943
17	2	0.0188	0.2971
17	3	0.0074	0.2943
19	2	0.0220	0.2967
19	3	0.0101	0.2937

Table 6: Comparison between the natural frequencies and the damping ratios of the experiment, the polynomial model, and the interpolation model.

	z_1	f_1 (Hz)	ζ_1	z_3	f_3 (Hz)	ζ_3
experiment	-1.21	8.5	0.0158	0.77	7.7	0.0145
cubic model	-1.43	5.70	0.0038	0.96	5.11	0.0043
interpolation model	-1.17	8.67	0.0034	0.77	9.16	0.0032

the stable equilibria with small-motion properties of the experiment, and also by comparing numerical simulations with the experiment. After discussing damping issues, we evaluate the identified vector fields themselves.

4.1. Estimation of Natural Frequencies and Damping Ratios

Linearizing the identified polynomial model of equations (6) and (7) around the equilibrium points, we can calculate the eigenvalues of the linearized model, and hence estimate the natural frequencies and damping ratios for comparison with experimental measurements. Using the cubic model based on $n = 3$ harmonics and thirty UPOs, the equilibrium points are estimated to be $z_1 = -1.4260$ V, $z_2 = -0.1000$ V, and $z_3 = 0.9639$ V, at which the cubic stiffness function is zero to four decimal places. These values can be compared to the experimental stable equilibria of -1.21 V and 0.77 V.

The eigenvalues of the Jacobian of equation (6) are computed as $-0.0029 \pm 0.7605i$, for z_1, -0.5102 and 0.5045 for z_2, and $-0.0029 \pm 0.6812i$ for z_3 in the time-normalized system. As expected, z_1 and z_3 are stable spirals, and z_2 is a saddle. For the spirals, the real part represents the decay rate, and the imaginary part represents the damped natural frequency. The damping ratio can be estimated by dividing the real part by the imaginary part, yielding $\zeta_1 = 0.0038$ and $\zeta_3 = 0.0043$ for z_1 and z_3 respectively. Converting to real time by multiplying by the driving frequency (7.5 Hz in this case), the damped natural frequencies are $f_1 = 5.7037$ Hz and $f_3 = 5.1090$ Hz, respectively.

The same analysis can be performed on the interpolation model, which is continuous and has a well defined derivative except on a measure-zero set of grid points. For the time-normalized model based on 15 interpolation functions, the predicted fixed points are $z_1 = -1.1731, z_2 = -0.2172$, and $z_3 = 0.7699$, with z_1 and z_3 representing stable spirals, and z_2 being a saddle. The associated natural frequencies and damping ratios are $\zeta_1 = 0.0034$ and $f_1 = 8.6685$ Hz for z_1, and $\zeta_3 = 0.0032$ and $f_3 = 9.1568$ Hz for z_3.

The transfer functions of the experimental system were obtained for small free motions about each stable equilibrium. Using the half-power point method, and assuming the damping ratio, ζ, is small, the damping ratio can be estimated. Table 6 contains a comparison of the natural frequencies and the damping ratios of the two linearized models and the experimental small-motion transfer functions.

The cubic model resulted in under-estimated frequencies, where as the interpolation model resulted in slightly over-estimated frequencies.

The discrepancies between the measured natural frequencies and those predicted by the identified models may not be so surprising. The parameters were identified by minimizing

the squares of errors in the nonlinear functions (in terms of their Fourier harmonics), but not by minimizing the squares of errors in the *slopes* of these functions, whence the linearized properties are derived. Magnetic forces are inversely proportional to distances squared, and the polynomial model contains no such terms. Local variations in slopes may deviate considerably, as can be imagined from the deviations between the stiffness characteristics of the polynomial and interpolation models (Figure 3).

Both models produced damping factors that are lower than the small-motion linear damping estimates. We will return to this damping issue shortly.

4.2. Numerical Simulations

Numerical integration of equation (6) is carried out using a Runge-Kutta method. The phase portrait of the experiment, plotted using a finite difference approximation to the experimental velocity, such that $\dot{z}_i \approx (z_{i+1} - z_{i-1})/2h$, along with the phase portraits of the simulated cubic and interpolation models, are shown in Figures 5-7. The numerical derivative is trusted because numerical derivatives plotted in the simulated cases were not visually distinguishable in the phase portraits. Both simulated models reproduce the qualitative feel of the experimental plot, in that they all exhibit random-like walks between the wells, intermixed with orbits surrounding both wells, at similar scales of global motion. The visibly noteworthy distinction is in the depth of the dips the trajectories make as they pass by the saddle ($z \approx 0$). The experimental dips are more pronounced than the cubic model, and similarly pronounced as in the interpolation model. Dips are again tied to the extremity of the features of the potential wells. If an unforced vibration were considered, the cubic wells, being smoothed over compared to the interpolation wells (and probably compared to reality) such that the local maximum of the saddle is lower than in the interpolation model, would allow larger kinetic energies in the vicinity of the saddle, and hence larger velocities such that the dips are less pronounced. This qualitative feature is likely to carry over in the presence of harmonic forcing. The pronounced dips are seen in other experiments on magneto-elastic two-well oscillators (e.g. Moon [27]).

Periodic orbits were extracted from the pseudo phase spaces of the simulations, under the same reconstruction parameters as in the experimental extractions. Plots of selected periodic orbits are displayed in the experiment (Figure 8), cubic model (Figure 9), and interpolation model (Figure 10). The comparison of the extracted orbits might be extrapolated by suspecting the existence of nearly symmetric sets of unstable periodic orbits. Since the nonlinear stiffness is not purely symmetric, it is conceivable that the broken symmetry might annihilate some of the symmetries suspected in the response. Some symmetries are evident among those extracted. While the agreement in the extracted periodic orbits varies, we should note that large differences in extracted orbits does not exclude the existence of more similar orbits that may not have been visited in the finite-length responses. Both the cubic and interpolation models qualitatively support the experiment, with more striking matches witnessed in the interpolation model.

Finally, we looked at Poincaré sections of the data. The Poincaré sections from the experiment, the cubic model, and the interpolation model are compared in Figure 11. Both models are quite cloudy compared to the experiment; the models do not reveal any localized or layered structure that the experimental data exhibits. This suggests that the models indeed have under estimated damping [28, 29]. Localized layering is associated with phase volume contraction, which is usually related to damping.

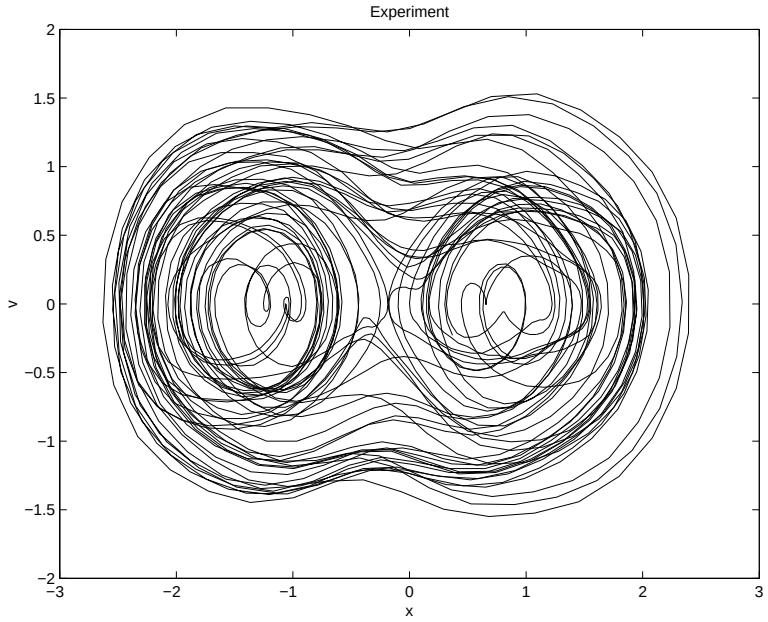

Figure 5: A phase portrait from the experimental data.

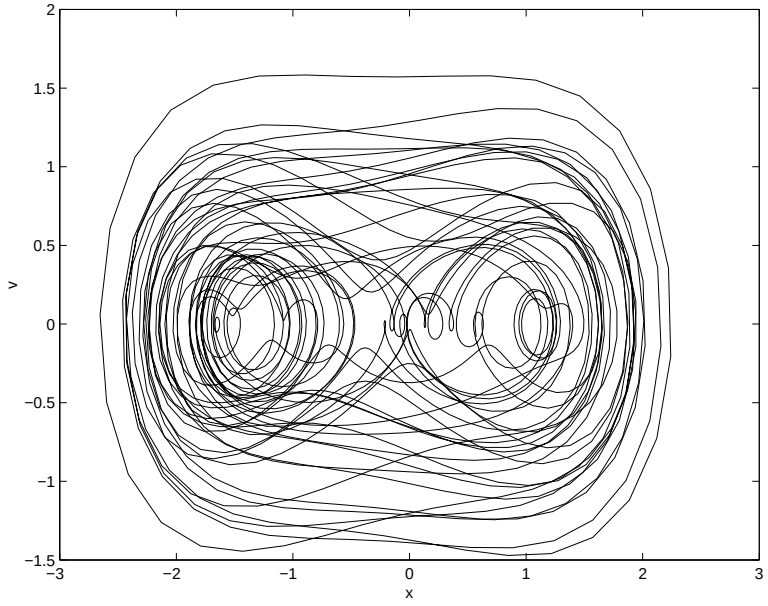

Figure 6: A phase portrait from the simulated cubic model.

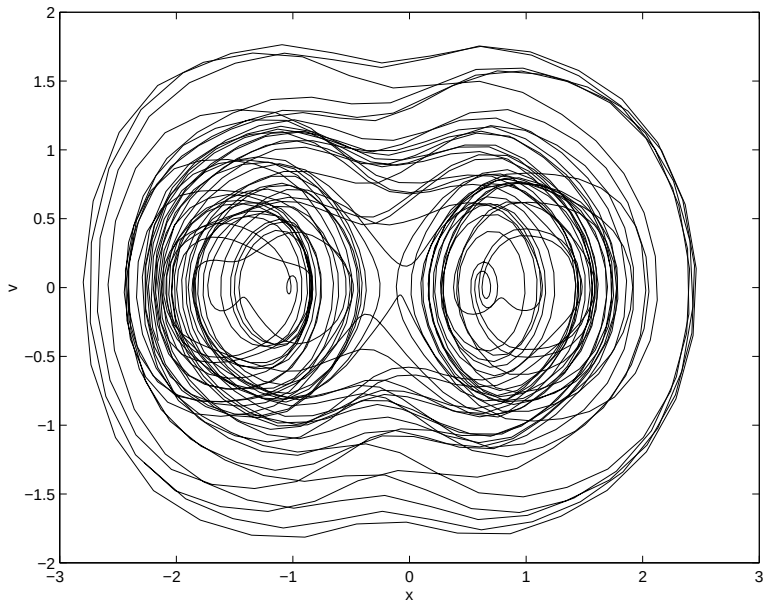

Figure 7: A phase portrait from the simulated interpolation model.

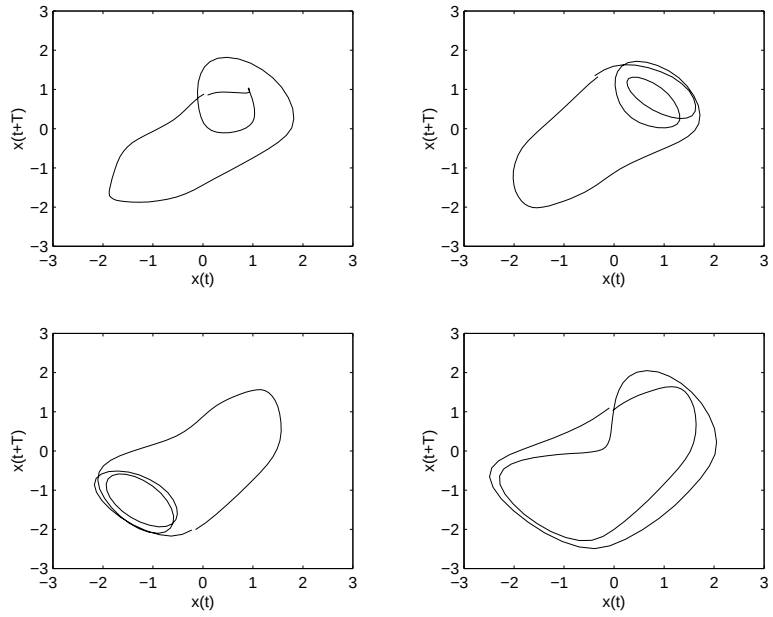

Figure 8: Some extracted period-four orbits from the experimental data.

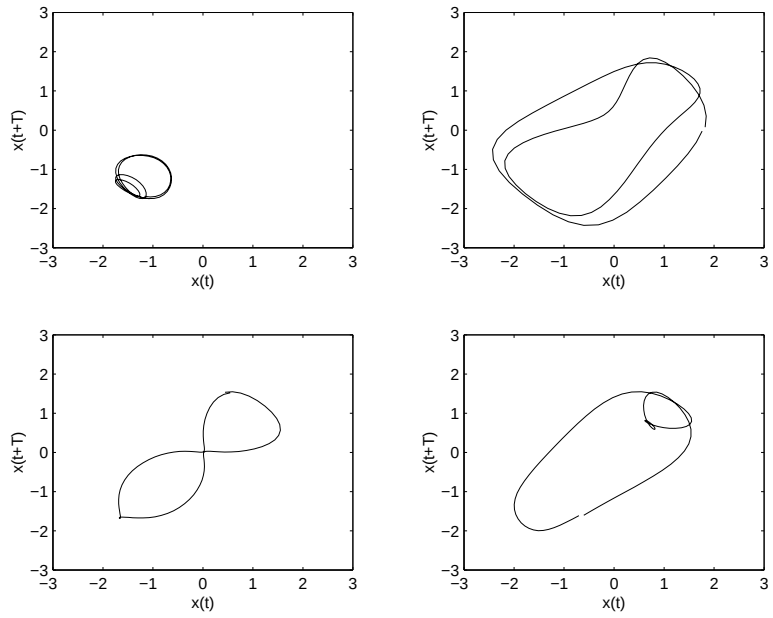

Figure 9: Some extracted period-four orbits from the simulated cubic model.

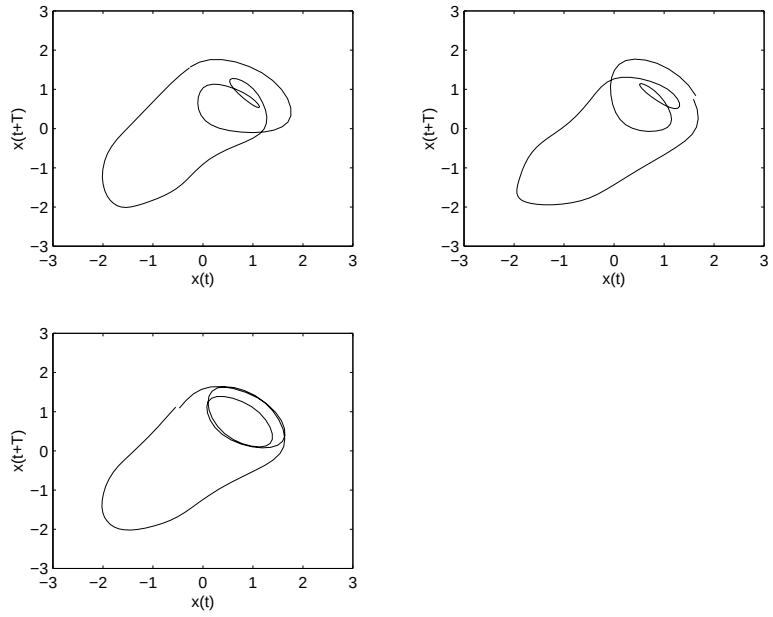

Figure 10: Some extracted period-four orbits from the simulated interpolation model.

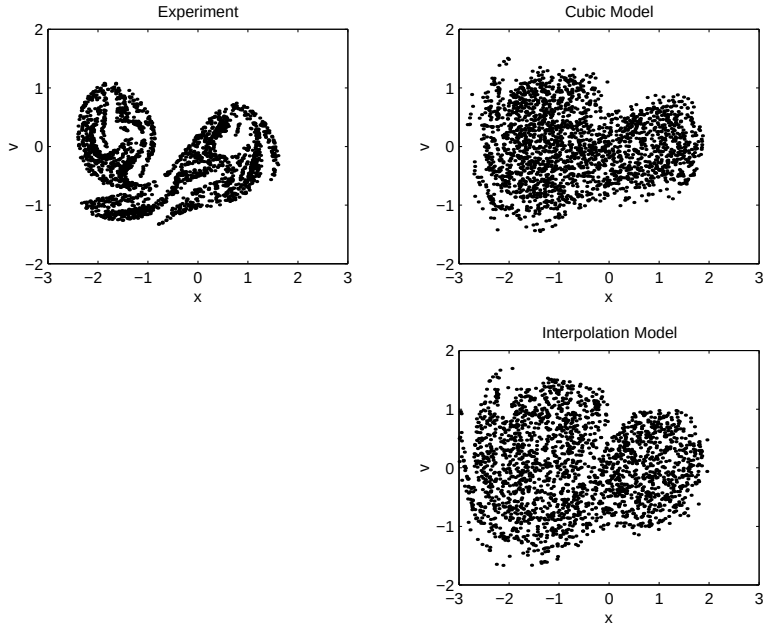

Figure 11: The Poincaré sections from the experiment, cubic model, and interpolation model are shown on the upper left, upper right, and lower right.

As a cautionary note, the post homoclinic-bifurcation behavior of the two-well oscillator, or any chaotic system, can be rather complicated, with windows of higher-period motions amidst intervals of chaotic behavior. The identification method makes use of the existence of periodic solutions and the magnitudes and phases of its harmonics, and not their stabilities. It is conceivable for the identified polynomial model to contain periodic orbits close to those used in the identification, but with one of them turning out to be stable. If this were to happen, such a simulated stable periodic response might, at first glance, appear strikingly different from the experimental chaotic response, when in fact the model may otherwise be a good fit of the experimental system.

4.3. Identification with Damping Known a Priori

Both the behavior localized to the equilibria and the global responses as viewed in the Poincaré sections suggest that the harmonic balance method has produced under-estimated damping factors. And of the source of the under-estimated damping? One possible explanation is that the method has a weakness in determining damping estimates. Another possibility is that the incorporation of solely linear damping in the model is inaccurate. A third possibility is that there is an undetected bug in our computer program which only affects the damping estimates. In this section, we assume the former, and revisit the identification.

With a slight adjustment in the parameter identification scheme, we can incorporate a known damping coefficient into the algorithm. We do this by multiplying the harmonics of the $\dot{x}_k$ terms in the matrix $\mathbf{A}$ and including them in the known vector $\mathbf{q}$. The rest of the parameters are identified as before.

To this end, we have included a damping coefficient $\tilde{\alpha} = 0.0327$. The resulting identified cubic model and interpolation model have insignificant changes in the identified stiffness, but

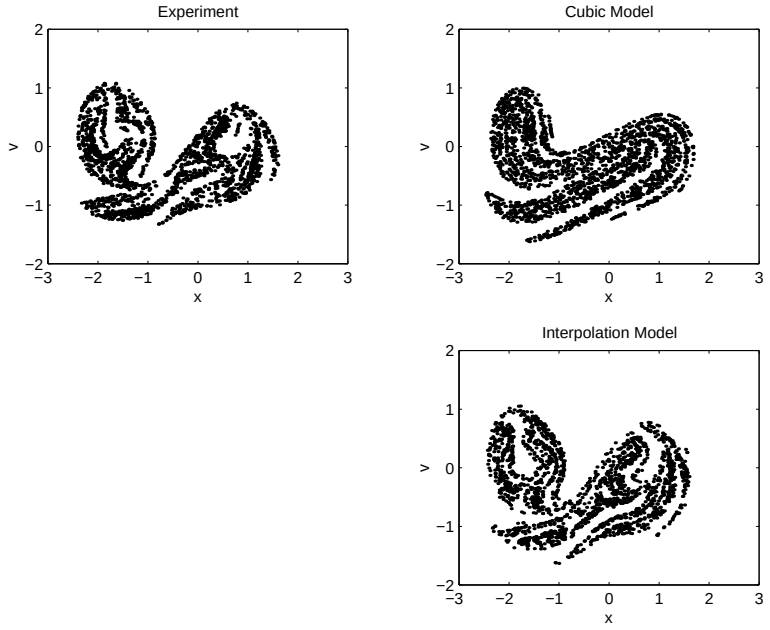

Figure 12: The Poincaré sections from the experiment, cubic model, and interpolation model are shown on the upper left, upper right, and lower right. The models were identified with the linear damping incorporated *a priori.*

the identified excitations are changed slightly, presumably to accommodate an energy balance. These identified models were simulated and the Poincaré sections are shown in Figure 12. The degree of foliation, or the visual amount of localized and layered features, between the experiment and the models is now comparable. Furthermore, the shape of the attracting set of the interpolation model matches up visually with the experiment better than the cubic model. The conclusions we draw from these simulations are, first, that the linearly estimated damping is a reasonable estimate, and second, that the interpolation model does an excellent job of modeling the nonlinear stiffness.

In this example, the harmonic balance method shows a weakness in evaluating linear damping. It is unknown whether this weakness prevails under nonlinear damping conditions. When we applied the harmonic balance we took advantage of linear damping by representing the z' harmonics through the derivatives of z in the Fourier series. If the system were to have nonlinear damping, we would need to estimate the z' time signal, evaluate the nonlinear damping form, and then find its Fourier coefficients.

4.4. Evaluating the Vector Field

In the previous sections we have evaluated the identified models by looking at linearized quantities and also by examining simulated responses. Linearized quantities do not fully represent a nonlinear system. The use of simulated responses may be risky in systems with sensitivity to parameters or initial conditions. However, an evaluation of the vector field itself should not have either of these problems.

The vector field is alternatively defined by the ordinary differential equation, which could

be represented in the form

$$z'' = g(z, z', \tilde{t}), \tag{8}$$

where $g(z, z', \tilde{t}) \approx g_m(z, z', \tilde{t})$, $g_m(z, z', \tilde{t})$ being the identified model of the forces in the oscillator. Thus, the function $g_m(z, z', \tilde{t}) = -\alpha z' - \sum_{i=0}^{p} \beta_i f_i(z, z') + a\cos\tilde{t} + b\sin\tilde{t}$ could consist of polynomial terms, interpolation functions, or other functions depending on the identification performed.

We check the quality of the model by evaluating the model at points in the experimental data. In other words, we check

$$z'' - g_m(z, z', \tilde{t}) = r,$$

where r is the error, and hope that r is small. In doing this, we approximate z' and z'' by finite differences.

We can make these vector field evaluations for any sequence of points in the data. We present results for some of the extracted UPOs. Figure 13 shows an example of the deviation, during an extracted period-four motion, between z'' and $g_m(z, z', \tilde{t})$ for the interpolation model and the cubic model, both of which include damping as determined *a priori*. The solid lines show the finite-difference acceleration, and the dashed lines track the identified force term. The dotted lines show the error. The interpolation model very accurately represents the forces in the oscillator. These trends are repeated in other extracted UPOs.

Figure 14 compares the normalized root mean squared errors for eight different UPOs, quantifying the finer capability of the interpolation model for capturing the system forces. The error is normalized against the root mean squared acceleration.

Finally, Figure 15 shows the normalized root mean squared error for the interpolation model with damping identified in the two ways discussed previously. The circles represent the model with damping identified from small-motion linear behavior, and the asterisks track the case of damping found by balancing harmonics. The differences in the vector-field errors are small, but the model with *a priori* linear damping consistently out performs the model with damping found by the harmonic-balance scheme.

5. Conclusion

The harmonic balance identification procedure has been applied for the parametric identification of a chaotic single degree of freedom oscillator, in which the the parameters appear linearly in the differential equation of motion. Many unstable periodic orbits are extracted from a single set of experimental data, and then used for the harmonic balance.

Quality of the results depends on the choice of the model. We see in this work how two different models, a polynomial model and an interpolation model, perform in approximating the experimental system in both its simulated global dynamics and in its linearized properties near equilibria. In this case, the interpolation model was better in representing the equilibria positions, the local frequencies, and the shape of the strange attracting set. The interpolation model also captured the nonlinear forces more accurately, as shown in vector-field evaluations. The interpolation model was likely to have traced the contours of the nonlinear stiffness better than the cubic model, while the cubic model was likely to smoothly fit the real characteristic. However, the cubic model was qualitatively satisfactory, and would lend itself better to analyses and parameter studies than the more complicated interpolation model.

In this example, the harmonic balance identification method was rather robust with respect to the number of harmonics balanced, the set of extracted periodic orbits, and the number

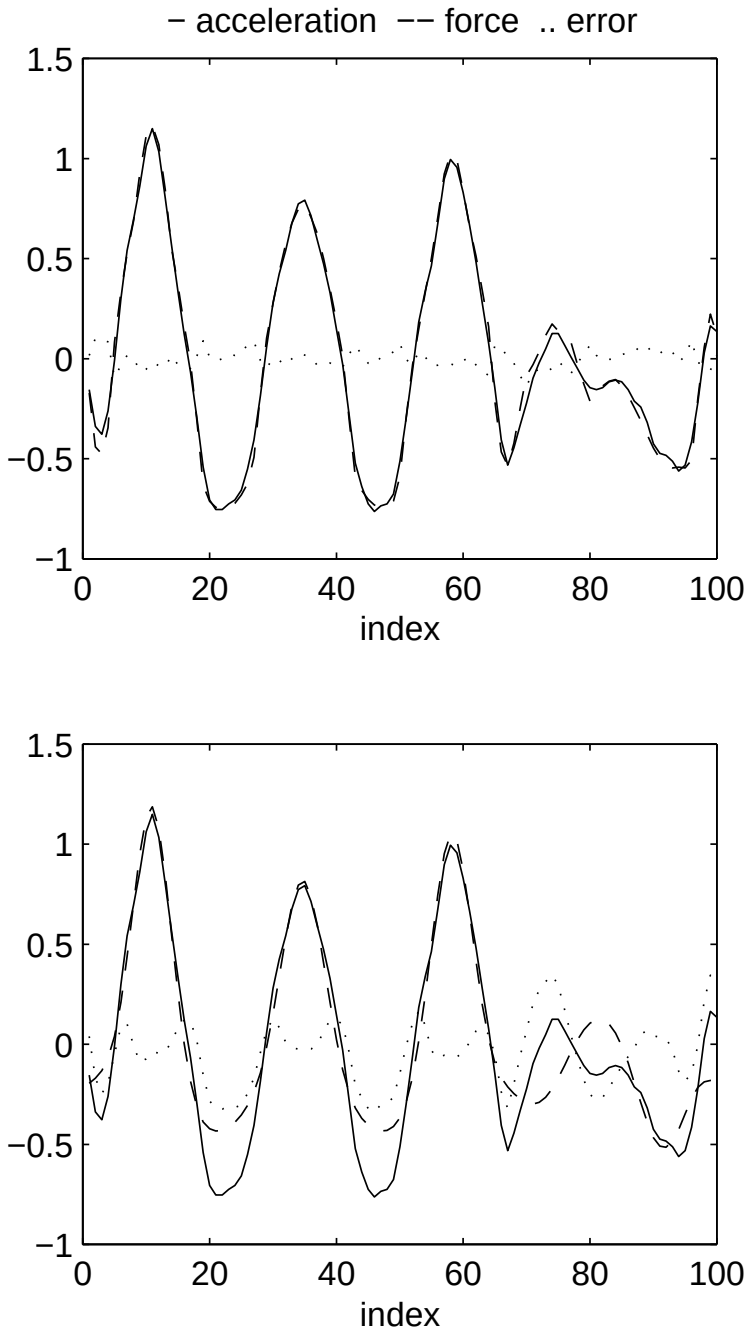

Figure 13: For a period-four orbit extracted from the experimental data, the solid line shows the acceleration, the dashed line follows the force evaluated in the models, and the dotted line indicates the error. The top figure is for the interpolation model, and the lower figure is for the cubic model.

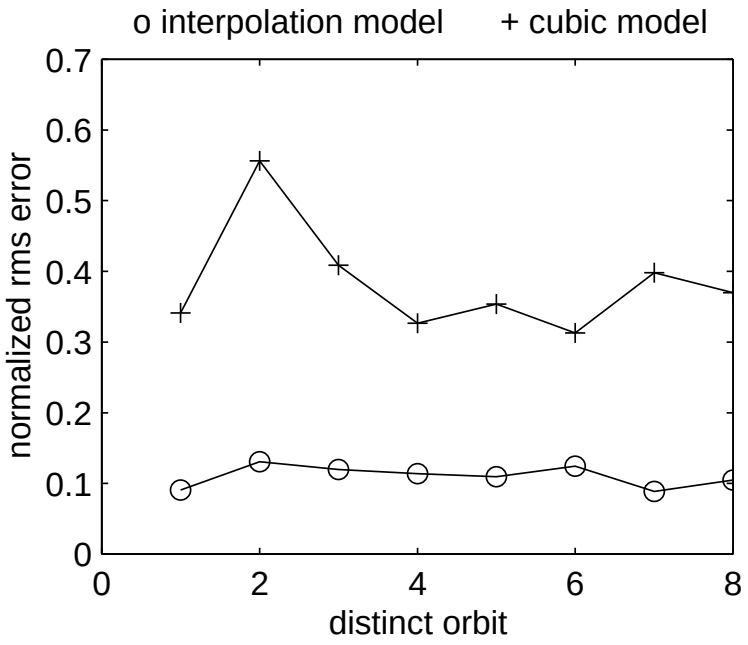

Figure 14: The normalized root mean squared errors in the interpolation model and the cubic model for eight different extracted UPOs.

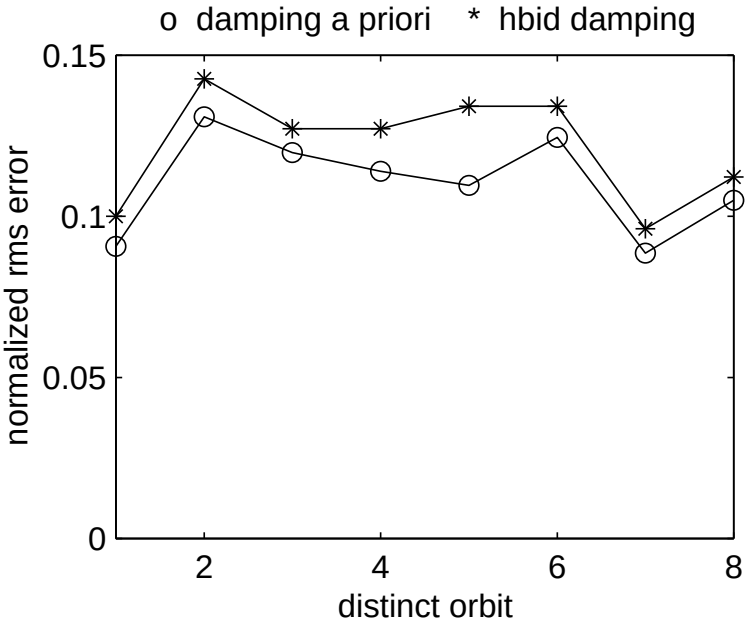

Figure 15: The normalized root mean squared errors in the interpolation model for eight different extracted UPOs. The plot compares the vector fields in the cases of damping estimated by linear dynamics and by balancing harmonics.

of interpolation functions. While the harmonic balance identification method successfully identified the nonlinear stiffness, there was some deviation in the damping estimation which affected details in the simulated dynamics, such as in the degree of phase-space contraction visible in the Poincaré section. This effect of damping estimation on the vector-field root mean squared error was slight, but it was consistent across segments of the data series.

For assessing the feasibility of harmonic balance identification in chaotic systems, future work might address systems with clearly defined nonlinearity, and in multi-degree-of-freedom systems.

Acknowledgement Author CMY was supported by CSIST of Taiwan.

6. *

References

[1] A. H. Nayfeh 1985 *Computers and Structures* **20**, 487-493. Parametric identification of nonlinear dynamic systems.

[2] G. Stry and D. J. Mook 1992 *Nonlinear Dynamics* **3**, 1-11. An experimental study of nonlinear dynamic system identification.

[3] O. Gottlieb and M. Feldman 1997 *Journal of Offshore Mechanics and Arctic Engineering* **119** 239-243. Application of a Hilbert-transform based algorithm for parameter estimation of a nonlinear ocean system roll model.

[4] M. Feldman 1997 *Journal of Sound and Vibration* **208** (3) 475-489. Nonlinear free vibration identification via the Hilbert transform.

[5] K. Yasuda, S. Kawamura, and K. Watanabe 1988a *JSME International Journal, Series III,* **31**, 8-14. Identification of nonlinear multi-degree-of-freedom systems (presentation of an identification technique).

[6] K. Yasuda, S. Kawamura, and K. Watanabe 1988b *JSME International Journal, Series III,* **31**, 302-309. Identification of nonlinear multi-degree-of-freedom systems (identification under noisy measurements).

[7] H. D. I. Abarbanel, R. Brown, J. Sidorowich, and L. Tsimring 1993 *Reviews of Modern Physics* **65**, 1331-1392. The analysis of observed chaotic data in physical systems.

[8] N. B. Tufillaro, T. Abbott, and J. Reilly 1992 *An Experimental Approach to Nonlinear Dynamics and Chaos,* Addison-Wesley.

[9] D. Auerbach, P. Cvitanovic, J.-P. Eckmann, G. Gunaratne, and I. Procaccia 1987 *Physical Review Letters* **58**, 2387-2389. Exploring chaotic motion through periodic orbits.

[10] D. P. Lathrop and E. J. Kostelich 1989 *Physical Review A* **40**, 4028-4031. Characterization of an experimental strange attractor by periodic orbits.

[11] S. Hammel and J. Heagy 1992 abstracts of the *SIAM Conference on Applications of Dynamics Systems,* Snowbird, Utah, October 15-19. Chaotic system identification using linked periodic orbits.

[12] R. V. Kesaraju and S. T. Noah 1994 *Nonlinear Dynamics* **6**, 433-457. Characterization and detection of parameter variations of nonlinear mechanical systems.

[13] N. Van de Wouw, G. Verbeek, and D. H. Van Campen 1995 *Journal of Vibration and Control* **1**, 291-305. Nonlinear parametric identification using chaotic data.

[14] C.-M. Yuan and B. F. Feeny 1998 *Journal of Vibration and Control* **4** (4), 405-426. Parametric identification of chaotic systems.

[15] F. Takens 1981 *Dynamical Systems and Turbulence,* D. A. Rand and L.-S. Young, eds. (Warwick 1980) *Lecture Notes in Mathematics* **898** 366-381, Springe-Verlag, Berlin.

[16] N. H. Packard, J. P. Crutchfield, J. D. Farmer, and R. S. Shaw 1980 *Physical Review Letters* **45** (9) 712-716. Geometry from a time series.

[17] J. P. Cusumano and B. Kimble 1994 *Nonlinearity and Chaos in Engineering Dynamics,* J. M. T. Thompson and S. R. Bishop, eds., John Wiley and Sons, Chichester, 71-89. Experimental observation of basins of attraction and homoclinic bifurcation in a magneto-mechanical oscillator.

[18] A. M. Fraser and H. L. Swinney 1986 *Physical Review A* **33** (2), 1134-1140. Independent coordinates for strange attractors from mutual information.

[19] D. S. Broomhead and G. P. King 1986 *Physica D* **20**, 217-236. Extracting qualitative dynamics from experimental data.

[20] M. Kennel, R. Brown, and H. D. I. Abarbanel 1992 *Physical Review A* **45**(6) 3403-3411. Determining embedding dimension for phase-space reconstruction using geometrical construction.

[21] Z. Al-Zamel 1999 *Unstable Periodic Orbit Extraction Error and its Effect on Nonlinear System Parametric Identification,* PhD Thesis, Michigan State University, East Lansing.

[22] K. Yasuda and S. Kawamura 1989 *JSME International Journal, Series III*, **32** (3) 365-372. A nonparametric identification technique for nonlinear vibratory systems.

[23] K. E. Atkinson 1989 *An Introduction to Numerical Analysis,* second edition, John Wiley and Sons, 1989.

[24] G. Strang 1976 *Linear Algebra and its Applications,* Academic Press, New York.

[25] R. E. Mickens 1988 *Journal of Sound and Vibration* **124**, 199-203. Bounds on the Fourier Coefficients for the periodic solutions of nonlinear oscillator equations.

[26] Z. Al-Zamel 1999 *Unstable Periodic Orbit Extraction Error and its Effect on Nonlinear System Parametric Identification,* PhD Thesis, Michigan State University, East Lansing.

[27] F. C. Moon 1987 *Chaotic Vibrations*, Wiley–Interscience, New York.

[28] F. C. Moon 1980 *Journal of Applied Mechanics* **47** 638-644. Experiments on chaotic motions of a forced nonlinear oscillator: strange attractors.

[29] R. H. Dowell and C. Pezeshki 1986 *Journal of Applied Mechanics* **53** 5-9. On the understanding of chaos in Duffing's equation including a comparison with experiment.